ISSN 1674-1056
http://cpb.iphy.ac.cn
http://iopscience.iop.org/cpb
中国物理 B
Chinese Physics
中国物理
Chinese Physics B

Role of Bloch oscillation in high-order harmonic generation from periodic structure

Lu Liu(刘璐), Jing Zhao(赵晶), Jian-Min Yuan(袁建民), Zeng-Xiu Zhao(赵增秀)
Citation: Chin. Phys. B . 2019, 28(11): 114205 . **doi:** 10.1088/1674-1056/ab47f7
Journal homepage: http://cpb.iphy.ac.cn; http://iopscience.iop.org/cpb

What follows is a list of articles you may be interested in

Resolving multi-orbital effects on high harmonic generation from aligned N_2 molecules in linearly and elliptically polarized intense laser fields

Hong-Jing Liang(梁红静), Xin Fan(范鑫), Shuang Feng(冯爽), Li-Yu Shan(单立宇), Qing-Hua Gao(高庆华), Bo Yan(闫博), Ri Ma(马日), Hai-Feng Xu(徐海峰), Da-Jun Ding(丁大军)
Chin. Phys. B . 2019, 28(9): 094211 . **doi:** 10.1088/1674-1056/ab3440

Quantum interference of multi-orbital effects in high-harmonic spectra from aligned carbon dioxide and nitrous oxide

Hong-Jing Liang(梁红静), Xin Fan(范鑫), Shuang Feng(冯爽), Li-Yu Shan(单立宇), Qing-Hua Gao(高庆华), Bo Yan(闫博), Ri Ma(马日), Hai-Feng Xu(徐海峰)
Chin. Phys. B . 2019, 28(9): 094207 . **doi:** 10.1088/1674-1056/ab3438

Femtosecond enhancement cavity with kilowatt average power

Jin Zhang(张津), Lin-Qiang Hua(华林强), Shao-Gang Yu(余少刚), Zhong Chen(陈忠), Xiao-Jun Liu(柳晓军)
Chin. Phys. B . 2019, 28(4): 044206 . **doi:** 10.1088/1674-1056/28/4/044206

Effect of multiple rescattering processes on harmonic emission in spatially inhomogeneous field

Cai-Ping Zhang(张彩萍), Chang-Long Xia(夏昌龙), Xiang-Fu Jia(贾祥富), Xiang-Yang Miao(苗向阳)
Chin. Phys. B . 2018, 27(3): 034206 . **doi:** 10.1088/1674-1056/27/3/034206

Spectral redshift of high-order harmonics by adding a weak pulse in the falling part of the trapezoidal laser pulse

Xue-Fei Pan(潘雪飞), Jun Zhang(张军), Shuai Ben(贲帅), Tong-Tong Xu(徐彤彤), Xue-Shen Liu(刘学深)
Chin. Phys. B . 2018, 27(2): 024206 . **doi:** 10.1088/1674-1056/27/2/024206

SPECIAL TOPIC — Strong-field atomic and molecular physics

Role of Bloch oscillation in high-order harmonic generation from periodic structure*

Lu Liu(刘璐)[1], Jing Zhao(赵晶)[2], Jian-Min Yuan(袁建民)[1,2], and Zeng-Xiu Zhao(赵增秀)[2,†]

[1] Graduate School of China Academy of Engineering Physics, Beijing 100193, China

[2] Department of Physics, College of Liberal Arts and Science, National University of Defense Technology, Changsha 410073, China

(Received 30 July 2019; revised manuscript received 23 September 2019; published online 1 November 2019)

The high-order harmonic generation from a model solid structure driven by an intense laser pulse is investigated using the semiconductor Bloch equations (SBEs). The main features of harmonic spectrum from SBEs agree well with the result of the time-dependent Schrödinger equation (TDSE), and the cut-off energy can be precisely estimated by the recollision model. With increasing the field strength, the harmonic spectrum shows an extra plateau. Based on the temporal population of electron and the time–frequency analysis, the harmonics in the extra plateau are generated by the Bloch oscillation. Due to the ultrafast time response of the Bloch electron, the generated harmonics provide a potential source of shorter isolated attosecond pulse.

Keywords: high-order harmonic generation, attosecond pulse, semiconductor Bloch equations, time-dependent Schrödinger equation

PACS: 42.65.Ky, 32.80.Rm, 42.65.Re **DOI:** 10.1088/1674-1056/ab47f7

1. Introduction

High-order harmonic generation (HHG) is a non-linear process when atoms, molecules, or plasmas[1–4] are illuminated by an intense laser pulse. HHG is a prerequisite of attosecond pulse[5] due to the coherent nature, which can also be used to investigate the ultrafast electronic dynamics in matters. HHG paves the way to new ultrafast imaging methods, such as molecular tomography and spectroscopy.[6,7] Recently, due to the specific properties of the electrons in semiconductor materials, more investigations have been focused on the rich high harmonics from solids. In present experiments, various crystals are exposed to the strong laser field, including ZnO,[8–10] GaSe,[11,12] SiO_2,[13,14] MgO,[15] MoS_2,[16] and even solid Ar, Kr.[17] Different forms of semiconductor materials ranging from bulk to monolayer[16,18,19] and quantum wires [20] are used to improve the efficiency of the harmonics from solids. By increasing the damage threshold and using the few-cycle intense field, HHG from solids is becoming another important source of extreme ultraviolet (EUV) emission.[14,21] It provides an efficient method to probe the crystal structure in momentum space[22,23] and real space,[15] and to investigate the electron dynamics.[8,9,11,13,16,17,24] At present, the mechanism of HHG from solids has aroused concern and extensively study, but there is still controversy.[9,25–30]

By analogy with HHG of atoms,[31,32] Vampa *et al.* propose a three-step model[9] to explain the mechanism of HHG from solids. Within the mean-field approximation, HHG from solids can be understood in the single-electron picture. The tunnel ionization in atoms from bound state to continuum state is replaced by ionization from the highest valence band (VB) to conduction band (CB) in solids. Then the ionization induced electron–hole pairs are accelerated respectively within CB and VB with nonlinear responses under the laser field, which are governed by the dispersion relations. Due to the polarization builded up between the CB and VB, the electron recombines into the hole state previously created in the VB, and high harmonics are emitted with cut-off energy equal to the band gap at the corresponding instantaneous crystal momentum.[33,34] The harmonic cut-off energy induced by the interband polarization is found as a linear function of the driven laser field strength.[33] Nevertheless, the recollision model induced cut-off energy is restricted to the maximum band gap between VB and CB.

In addition, Ghimire *et al.* propose a two-step model,[35] which only takes the single-band motion of electron into account. Except for the transition to the higher CB through interband Zener tunneling,[36,37] the electron can also be driven to the boundary of the Brillouion zone (BZ), and then due to Bragg scattering, the electron performs periodic ballistic motion in momentum space accompanied by a real-space oscillation of the electron position, which is known as the intraband mechanism and called the Bloch oscillation (BO).[36,38] Under a time-dependent electric field $E(t)$, the BO period is $T_{\mathrm{B}} = 2\pi/\omega_{\mathrm{B}}(t)$ and the instantaneous Bloch frequency is

*Project supported by the NSAF, China (Grant No. U1730449) and the National Natural Science Foundation of China (Grant Nos. 11904341, 11774322, 91850201, and 11874066).

†Corresponding author. E-mail: zhaozengxiu@nudt.edu.cn

© 2019 Chinese Physical Society and IOP Publishing Ltd

$\hbar\omega_{\rm B}(t) = ea_0E(t)$,[39,40] where a_0 is the lattice constant. The electron momentum of intraband motion follows the acceleration law $\boldsymbol{k}(t) = \boldsymbol{k}_0 + e\boldsymbol{A}(t)$, where $\boldsymbol{k}_0$ is the initial momentum, and $\boldsymbol{A}(t)$ is the vector potential.[41,42]

Under an intense laser field, the translational invariance of a periodic structure is destroyed. The electron wave function becomes localized. The energy spectrum is discrete, which is called the Wannier–Stark ladder (WSL).[43–45] The eigenenergies are separated by the Bloch frequency $\omega_{\rm B}$. The real-space WSL is an equivalent picture of BO in momentum space, and they were firstly observed in the experiment on GaAs–GaAlAs superlattices [46] in 1988. However, because of the Zener tunneling,[36,37] the lattice vibration induced scattering of electrons, and doping scattering,[47,48] still there is no explicit measurement of BO in traditional solid structure. As the development of the femtosecond physics techniques, the BO can happen several times within one laser cycle, which is faster than the scattering. It is possible to detect the BO in semiconductor, and also the BO induced coherent radiation becomes a very promising source of the isolated attosecond pulse.

In fact, it is not sufficient to take only the recollision-electron (interband) or the BO-electron (intraband) emission into account, due to the strong coupling between the interband polarization and intraband current. In this work, we calculate the harmonic spectrum from a one-dimensional solid structure[37] using the semiconductor Bloch equations (SBEs)[37] which describe the coupled interband and intraband dynamics in a two-band model. While we use a few-cycle laser, the harmonic spectrum shows an obvious plateau, whose cut-off is limited by the maximum bandgap between the VB and CB, and the band structure information can also be reflected in the harmonic spectrum. The energy feature of the spectrum can be precisely estimated by the recollision-electron dynamics in real space.

When we increase the laser field, an extra plateau appears in the harmonic spectrum, whose cut-off is linearly dependent on the field strength.[49] The cut-off energy equals $N\omega_{\rm B}$, multiple integers of the Bloch frequency, and N is determined by the high frequency component of the band dispersion.[35] Based on the temporal population of electron and the time-frequency analysis, the second plateau is mainly contributed by BO-electron. The classical analysis based on ladder state in real space provides an explicit calculation of the cut-off energy in the extra harmonic plateau. The ultrafast dynamics of recollision-electron and BO-electron have been compared. The BO-electron dynamics can be controlled by the few cycle laser field shaping to synthesis an isolated attosecond pulse.

This paper is organized as follows. In Section 2, details of numerical method are presented. In Section 3, results of the emission are analyzed and discussed. The important results are summarized in Section 4. Atomic units $\hbar = m_0 = e = 1$ are used unless stated otherwise.

2. Method

2.1. Semiconductor Bloch equations

The band structure can be obtained by solving the following Schrödinger equation within single electron approximation:

$$\left[\frac{\boldsymbol{p}^2}{2m} + v(\boldsymbol{r})\right]\phi_{\boldsymbol{k}}^{\lambda} = \varepsilon_{\boldsymbol{k}}^{\lambda}\phi_{\boldsymbol{k}}^{\lambda}, \tag{1}$$

subjected to the periodic boundary condition $\phi_{\boldsymbol{k}}^{\lambda}(\boldsymbol{r}+\boldsymbol{L}) = \phi_{\boldsymbol{k}}^{\lambda}(\boldsymbol{r})$, where m is the mass of the electron and $\boldsymbol{L}$ corresponds to the macroscopic large size of the crystal. The periodic potential is given by $v(\boldsymbol{r})$ and $v(\boldsymbol{r}+\boldsymbol{a}_0) = v(\boldsymbol{r})$ with $\boldsymbol{a}_0$ being the lattice constant. According to the Bloch theorem, the Bloch function takes the form of

$$\phi_{\boldsymbol{k}}^{\lambda}(\boldsymbol{r}) = \mathrm{e}^{\mathrm{i}\boldsymbol{k}\cdot\boldsymbol{r}}u_{\boldsymbol{k}}^{\lambda}(\boldsymbol{r}), \tag{2}$$

with $u_{\boldsymbol{k}}^{\lambda}$ being a periodic function such that

$$u_{\boldsymbol{k}}^{\lambda}(\boldsymbol{r}+\boldsymbol{a}_0) = u_{\boldsymbol{k}}^{\lambda}(\boldsymbol{r}). \tag{3}$$

The eigenenergies $\varepsilon_{\boldsymbol{k}}^{\lambda}$ determines the dispersion relation between the electron energy and the crystal momentum $\boldsymbol{k}$ within the $\lambda^{\rm th}$ band. Subjected to an external time-varying laser field $E(t)$, the time evolution of the crystal momentum is governed by

$$\frac{\mathrm{d}}{\mathrm{d}t}\boldsymbol{k}(t) = -E(t). \tag{4}$$

A set of coupled differential equations which govern the coupled dynamics of electrons and holes under the optical polarization between different bands are called the semiconductor Bloch equations (SBEs). It is general to formulate the SBEs starting from a many-body approach within the two-band approximation. The Coulomb interaction among the photoexcited carriers in the regime of extremely nonlinear optics is very weak, and it is typically of order of the exciton binding energy. Therefore in this work the Coulomb interaction can be ignored. Both the optical interband polarization $p_{\boldsymbol{k}}$ and the occupation $n_{\boldsymbol{k}}^{\rm e(h)}$ of electron (hole) can be calculated by solving the following SBEs:

$$\begin{aligned}\mathrm{i}\hbar\frac{\partial}{\partial t}p_{\boldsymbol{k}} &= \left(\varepsilon_{\boldsymbol{k}}^{\rm e} + \varepsilon_{\boldsymbol{k}}^{\rm h} - \mathrm{i}\frac{\hbar}{T_2}\right) - \left(1 - n_{\boldsymbol{k}}^{\rm e} - n_{\boldsymbol{k}}^{\rm h}\right)d_{\boldsymbol{k}}E(t) \\ &\quad + \mathrm{i}eE(t)\cdot\boldsymbol{\nabla}_{\boldsymbol{k}}p_{\boldsymbol{k}}, \end{aligned}\tag{5}$$

$$\hbar\frac{\partial}{\partial t}n_{\boldsymbol{k}}^{\rm e(h)} = -2\mathrm{Im}[d_{\boldsymbol{k}}E(t)p_{\boldsymbol{k}}^{*}] + eE(t)\cdot\boldsymbol{\nabla}_{\boldsymbol{k}}n_{\boldsymbol{k}}^{\rm e(h)}, \tag{6}$$

where $\varepsilon_{\boldsymbol{k}}^{\rm e(h)}$ is the electron (hole) energy in the CB (VB). $d_{\boldsymbol{k}}$ is the dipole matrix element, which is related to the optical interband transition, while the term related to $\boldsymbol{\nabla}_{\boldsymbol{k}}$ represents the intraband excition. The energies and the dipole matrix elements are obtained from the Schrödinger equation in Eq. (1).

T_2 is the dephasing time of the polarization, which is taken as half of the driving laser optical period.[50]

The macroscopic current J and the polarization P induced by the the motion of electron (hole) within the bands are

$$P(t) = \sum_{\boldsymbol{k}} [d_{\boldsymbol{k}} p_{\boldsymbol{k}}(t) + \text{c.c.}], \tag{7}$$

$$J(t) = \sum_{\lambda,\boldsymbol{k}} e v_{\boldsymbol{k}}^{\lambda} n_{\boldsymbol{k}}^{\lambda}(t). \tag{8}$$

Here $v_{\boldsymbol{k}}^{\lambda} = \nabla_{\boldsymbol{k}} \varepsilon_{\boldsymbol{k}}^{\lambda}$ is the group velocity in λ^{th} band, which is proportional to the derivative of the dispersion with respect to $\boldsymbol{k}$. The high harmonic spectrum from the semiconductor structure can thus be obtained by

$$I(\omega) \propto |\omega^2 P(\omega) + \mathrm{i}\omega J(\omega)|^2, \tag{9}$$

where the interband and the intraband emissions are given by $I_{\text{pol}} = |\omega^2 P(\omega)|^2$ and $I_{\text{curr}} = |\omega J(\omega)|^2$, respectively.

2.2. Classical analysis

Besides the calculations in the momentum space, it is useful to investigate the interaction of solids with strong laser field in real space using classical analysis. In crystalline solids, an electron with momentum $\boldsymbol{k}$ tunnels vertically from the VB to CB around the peak of the laser field, and forms an electron–hole pair. The electron (hole) is subsequently accelerated in the corresponding CB (VB) and a classical trajectory is obtained according to the Newton equation. Based on Eq. (4), the momentum of the electron at time t after tunneling into the CB at time t' is determined by

$$\boldsymbol{k}(t) = \boldsymbol{A}(t) - \boldsymbol{A}(t'), \tag{10}$$

where $\boldsymbol{A}(t)$ is the vector potential of the laser field. The trajectories of the electron and the hole along their respective bands are determined by

$$x^{\text{e}} = \int_{t'}^{t} \nabla \varepsilon^{\text{e}}[\boldsymbol{k}(\tau)]\,\mathrm{d}\tau, \tag{11}$$

$$x^{\text{h}} = \int_{t'}^{t} \nabla \varepsilon^{\text{h}}[\boldsymbol{k}(\tau)]\,\mathrm{d}\tau. \tag{12}$$

After tunneling, when the electron and the hole meet again at time t_{r} in real space, the recombination gives rise to the emission of high harmonics. The resulted harmonic photon energy is thus given by

$$\hbar\omega = \varepsilon[\boldsymbol{k}(t_{\text{r}})] = \varepsilon^{\text{e}}[\boldsymbol{k}(t_{\text{r}})] - \varepsilon^{\text{h}}[\boldsymbol{k}(t_{\text{r}})]. \tag{13}$$

3. Results and discussion

We present the highest VB and the lowest CB involved in SBEs in Fig. 1(a), which are obtained by solving the single electron Schrödinger equation with a periodic model potential $V(x) = -0.37[1 + \cos(2\pi x/a_0)]$, where $a_0 = 8$ a.u. is the lattice constant. The corresponding minimum bandgap energy is 0.15 a.u., and the maximum bandgap energy is 0.51 a.u. We assume that the VB is initially fully occupied by electrons, while the CB is vacant. The laser pulse has a Gaussian profile with the full width at half maximum (FWHM) of $1T$, where T is the optical period, the laser strength maximum is 0.003 a.u., and the laser wavelength is 3200 nm. In Fig. 1(b), the harmonic spectrum obtained from the two-band SBEs agrees well with the spectrum from the full-band TDSE. However, under a stronger laser field, the results are not fit quite well with each other. In TDSE, we take all the bands involved. When driven to the boundary of the Brillouin zone, the electron can tunnel to a higher CB, and contribute to the harmonic emission. On the contrary, we ignore the contribution of higher CB in the two-band model, and focus on the Bloch oscillation electron. However, through proper selection of laser frequency and light intensity as well as specific solid materials, the contribution of high conduction band can be relatively suppressed in the experiment. So we use the SBEs with less involved bands to mimic the electron dynamics. The harmonic spectrum shows an obvious enhanced peak at the 10^{th} order. The corresponding energy labeled by vertical dashed lines exactly equals the minimum bandgap energy. The plateau ends at the 31^{st} order harmonic, which can be broadened linearly by increasing the laser field strength.

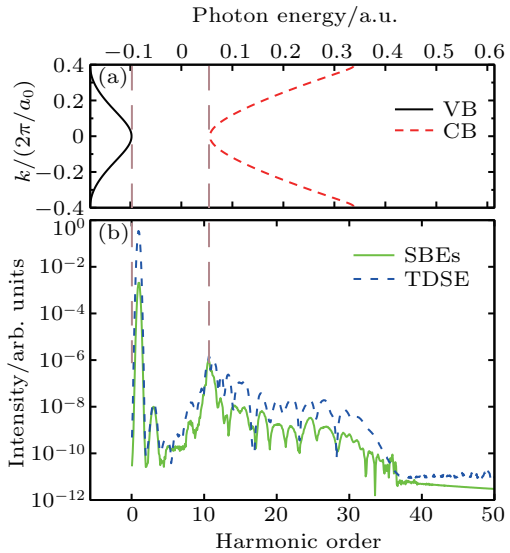


Fig. 1. (a) The highest VB and the lowest CB obtained from Schrödinger equation using the model potential. (b) High harmonic spectra obtained from SBEs (green line) including 2 bands, and TDSE (dashed blue line) including 18 bands. The laser field strength maximum is 0.003 a.u., and the wavelength equals 3200 nm. The vertical dashed lines denote the harmonic energy range corresponding to the minimum bandgap.

The dependence of the harmonic cut-off energies on the electric field strengths is shown with black circles in Fig. 2(b). The increase of cut-off energy ends at 36^{th} order, where the harmonic energy equals the maximum bandgap.

In order to investigate the relationship among the laser field strength, the cut-off energy, and the band structure, we use the recollision model proposed by Vampa[33] to investigate the electron dynamics in real space. In classical calculation, only one electron–hole pair is taken into account, the energies of electron and hole are obtained following the dispersion relationship with the laser strength maximum $E_0 = 0.003$ a.u. After created, based on Eqs. (11) and (12), the classical trajectories of electron and hole ionized at different time $t_1 = -0.5$ T and $t_2 = 0$ are represented by black lines and red lines respectively in Fig. 2(a). It shows that the electron and the hole are accelerated in the opposite directions in the real space. After drifting away for several lattices, the electron and the hole will recollision at t_r, which is indicated by the crossing of the black solid line and black dashed line, and emit a harmonic photon with energy being the difference between the VB and CB at $\boldsymbol{k}(t_r)$. The pair of electron and hole born at $t = 0$ shown with red lines cannot recollide with each other after drifted away, so they have no contribution to the recollision induced harmonics. The harmonic energies of the electron–hole pairs obtained from Eq. (13) are shown as functions of the creating time (green circles) and recombination time (blue diamonds) in the inset of Fig. 2(a). The cut-off energy of the classical results evaluated from the recollision model agrees well with the harmonic cut-off energy obtained from SBEs in Fig. 1(b).

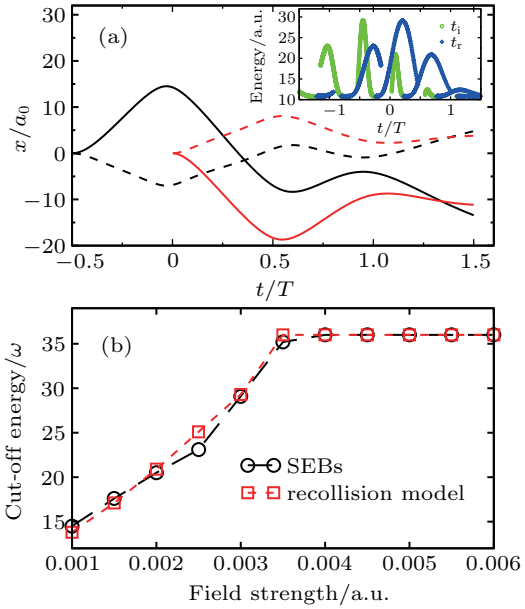


Fig. 2. (a) The classical trajectories of electrons (solid lines) and holes (dashed lines) created at $t_1 = -0.5T$ (black lines) and $t_2 = 0$ (red lines). The inset shows the electron energies corresponding to the ionization time (the green circles) and the recollision time (the blue diamonds) obtained from the classical analysis. (b) The harmonic cut-off linear laws of the first plateau, which are obtained from the SBEs calculation (black circles) and the recollision model (red squares).

Changing the field strength, we obtain the cut-off energies from the recollision model, which are shown with the red squares in Fig. 2(b). From $E_0 = 0.001$ a.u. to $E_0 = 0.0035$ a.u., the cut-off position reflects the dispersion relationship, which is nearly linear in the half of the parabolic-shape BZ. When the field strength increases beyond 0.0035 a.u., the cut-off energy reaches a maximum and remains a constant. They are consistent with the results from the SBEs in black circles in Fig. 2(b). Under a lower laser strength, the harmonics are generated from the recollision model, and the cut-off energy is restricted to the maximum bandgap of the two-band structure. This is different with the ionized electron in atomic system, whose maximum emission energy is unlimited.

An extra plateau will appear if the field strength continues to increase. Due to the short pulse duration of the few-cycle laser field we use, the material damage threshold can be shifted to higher intensity. According to Ref. [8], the highest vacuum laser field strength in their experiment is about 0.012 a.u. We calculate the harmonic spectra of $E_0 = 0.01$ a.u., 0.011 a.u., 0.012 a.u., as shown in Fig. 3. The Hanning window function[27,34] is used to filter the current signal and remove the non-physical background emission. It makes the extra plateau prominent, whose intensity is three orders lower than that of the first plateau. Dramatically, we find that these harmonic peaks are equally separated by the Bloch frequency.

In order to investigate the electron dynamics involved in the extra plateau, we show the temporal population of electron wave packet in the CB in Fig. 4(a). Initially, the electron wave packet is excited to the CB and leaves a hole in the VB with a high probability around $\boldsymbol{k} = 0$. Then the electron propagates along the quasi-momentum $\boldsymbol{k}$ in CB until it reaches the boundary of the BZ, and the Bragg scattering occurs. The electron wave packet shows up at the other direction of the BZ. We zoom in the region between two dashed lines in Fig. 4(a) from $-0.3T$ to $0.3T$, as shown in Fig. 4(b). The electron wave packet around the time $-0.2T$, $0.2T$, $-0.1T$, and $0.05T$ can be driven out of the edge and appear again in the other side of the BZ. Due to the time-dependent electric field strength, the Bloch frequency $\omega_B(t)$ is changing with time. It is important to find out the relation between $\omega_B(t)$ and the radiated harmonic energy.

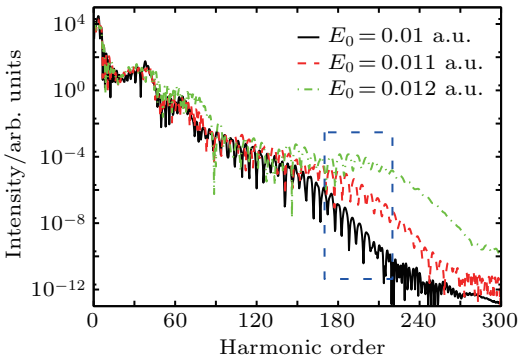


Fig. 3. The high harmonic spectra with the field strength maximum $E_0 = 0.01$ a.u. (black solid line), 0.011 a.u. (red dash line), 0.012 a.u. (dash dot line). The harmonics from 170th order to 220th order are highlighted by the blue dashed box.

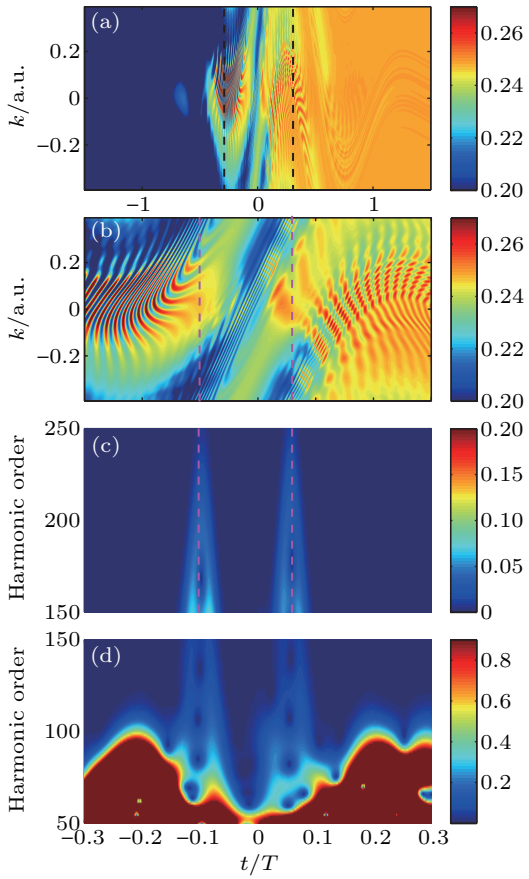


Fig. 4. (a) The temporal population of electron in CB in momentum space from $-1.5T$ to $1.5T$, when $E_0 = 0.012$ a.u. The zone in black dashed box is amplified in (b). (c), (d) The time–frequency analysis of harmonics from 50th order to 250th order with $E_0 = 0.012$ a.u. in Fig. 3.

We make the time–frequency analysis of the extra plateau of harmonic spectrum in Fig. 3 using wavelet window functions.[33,51] The time–frequency analysis result is exhibited in Figs. 4(c) and 4(d) corresponding to the low-frequency harmonics from 50th order to 150th order and the high-frequency harmonics from 150th order to 250th order. It shows that the harmonics from 50th order to 150th order in the extra plateau are mainly radiated at $-0.2T$ and $0.2T$. The higher-frequency harmonics with lower intensity from 150th order to 250th order are emitted around $-0.1T$ and $0.05T$ as shown with the dashed magenta lines. Compared with Fig. 4(b), the emission time of the harmonics in the extra plateau is the moment that the Bragg scattering occurs. This means that the high-frequency harmonics are contributed by the BO-electron. The higher $\omega_B(t)$, the higher harmonic energy radiated.

In connection with high harmonics released from molecule,[52] the electron dynamics from periodic structures can be studied in real space[40] based on the WSL state, which is an alternative description of BO in real space. For HHG from diatomic molecules, the electron localized in one of the potential wells can recombine not only with the original well, but also with the other one and release different harmonic energies. One possible trajectory is that electrons migrate between the laser field dressed potential wells, which contributes to harmonics with the energy difference between the two laser dressed wells E_0R, and R is the internuclear distance.

Analogously, for the carriers in the periodic potential subjected to an intense electric field, WSL states are formed[45] and the resulting eigenspectrum is discrete and equidistant, scaling linearly with the electric field strength. The energy difference between the neighboring states is E_0a_0. The strong field dressed localized electronic wavefunction has a long tail of the exponential decay spreading through several crystal sites. The electron can experience a long-distance transmission, which can be observed in the classical trajectories obtained from the classical analysis. When the electron furthest recombines to the N^{th} crystal site in the classical trajectories, the radiated cut-off energy of harmonic is $NE(t)a_0$. The cut-off energies estimated from classical analysis are represented with red squares in Fig. 5, which agree well with the simulation results from SBEs with black circles. Based on these analyses, the higher-order harmonic emission is closely related to the BO-electron, whose cut-off energy is proportional to the maximum number of the crystal sites that the electron migrates, and the instantaneous laser field strength.

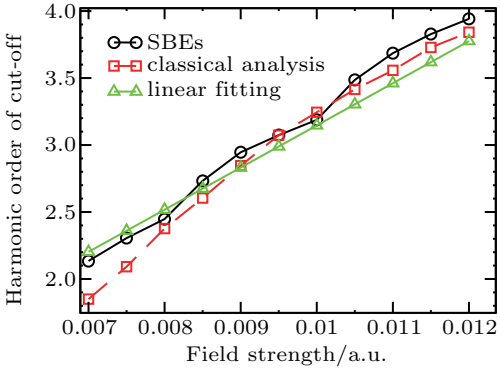


Fig. 5. The cut-off energy of the second plateau, which is linearly rising along with the increase of the field strength from 0.007 a.u. to 0.012 a.u.

Due to the BO-electron ultrafast dynamics in the extra harmonic plateau, the high harmonics generated from BO-electron could be the potential source of the isolated attosecond pulse. We show the attoseond pulses generated by 30 orders in the first harmonic plateau and the extra plateau in Fig. 6. The 754 as pulse generated from 10th order to 40th order harmonics showed in Fig. 6(a). Figure 6(b) shows the attoseond pulse with much shorter pulse width 251 as, which is generated by the harmonics from 120th order to 150th order. The lower-order harmonics in the first plateau, which is induced by the recollision model, emit twice per laser cycle like the atomic system. In contrast, the extra-plateau harmonics in higher order can emit several times within one cycle around the peak of the laser field. It shows that the sub-cycle BO electron emits the isolated attosecond pulse with much shorter pulse width than the recollision electron. The emission time of the attosecond pulse is the time when the Bragg scattering occurs. The BO electron emits the harmonics around the peak

of the single-cycle driven field. So we can use laser field shaping technology to control the sub-cycle dynamics of the BO electron and get a more effective attosecond pulse emission.

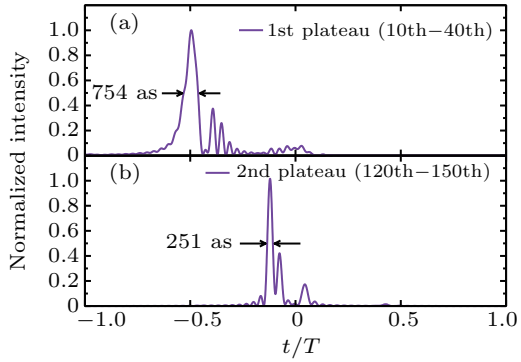


Fig. 6. The attosecond pulse synthesis (a) from 10th order to 40th order harmonics of the first plateau, and (b) from 120th order to 150th order harmonics of the second plateau.

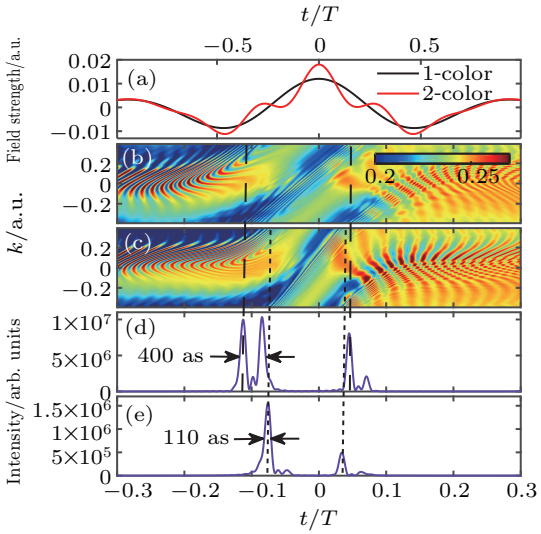


Fig. 7. (a) The 3200 nm laser field with black line, the 3200 nm + 1000 nm laser field with red thick line. The temporal population of electron in CB (b) under the 1-color laser field, and (c) under the 2-color laser field. The attosecond pulse synthesized from 100th order to 200th order harmonics in the 1-color laser field (d), and 2-color laser field (e).

We add a 1000 nm laser field with the FWHM of $1.875T$, and the field strength maximum is 0.006 a.u. The 2-color laser field is shown in Fig. 7(a) with the red thick line, and the field strength of the few-cycle laser around $t = 0$ is obviously increased. The electron wave packet can be accelerated from one side of the BZ to the other with a higher frequency and a shorter time. In Fig. 7(b), two consecutive Bragg scatterings occur around $t = -0.1T$ and $t = 0.05T$ under the 1-color laser field, which are marked by the dashed vertical lines. The instantaneous Bloch period is $0.15T$. However, in Fig. 7(c), the combined 2-color laser field makes the BO happen in a shorter duration $0.11T$, from $t = -0.08T$ to $t = 0.03T$, which are denoted by the dot vertical lines. So we can compress the harmonics in a wider frequency range from 100th order to 200th order in the extra plateau of the 2-color driven field to obtain a much shorter isolated attoseond pulse than that in the 1-color field. In Fig. 7(d), a 440 as pulse is obtained under the 1-color field, and the attosecond pulses are even not isolated. The emission time is the instants when the Bragg scattering occurs in Fig. 7(b). However, an 110 as isolated attoseond pulse is obtained from the 2-color laser field in Fig. 7(e). The two emission time of attosecond pulse is also the instants when the Bragg scatterings occur, which are indicated by the dashed lines in Fig. 7(c). This suggests that the generation of the intense isolated attosecond XUV pulse from the BO harmonics can be controlled by a multi-color laser field, like the atomic system.

4. Conclusion

We investigate the harmonic spectra from two-band SBEs and full-band TDSE, which agree well with each other. In the two-band model, the harmonic cut-off energy is limited by the bandgap between the two bands, and scales linearly with the field strength. The cut-off energy can be exactly estimated by the recollision model, which shows that the first plateau of the harmonics is produced by the recollision between the electron–hole pair. Increasing the field strength, we obtain an extra harmonic plateau, which shows the linear cut-off law with the field strength. When we compare the temporal electron population in momentum space with the time–frequency analysis, it shows that the time of higher-order harmonic emission is the moment when the Bragg scattering occurs. The harmonics in the extra plateau are induced by the BO-electron. We use an alternative description of BO, the WSL, to describe the mechanism of electron in real space. The trajectories of electrons in real space obtained from the classical analysis show that the electron can transit in the crystal sites of the WSL. The estimated cut-off energies from the representation in real space match well with the numerical results. The spectral width of the high-order harmonics is determined by the quiver distance of the electron in real space, which is related to the high frequency component of the dispersion. Then we take advantage of the ultrafast response of the BO-harmonics in the higher orders to obtain a 110 as isolated attosecond pulse in a 2-color laser field. BO-electron wave packet induced harmonic emission is a potential source of the shorter attosecond pulse generation.

In this model, the electrons are restricted within two bands, and the electrons undergo the Bloch oscillation instead of transiting to higher bands. We can realize the process in a realistic material, whose bandgap between the lowest and the second lowest conduction band is much higher than the bandgap between the first conduction band and the highest valence band.

References

[1] Ferray M, L'Huillier A, Li X F, Lompre L A, Mainfray G and Manus C 1988 *J. Phys. B* **21** L31
[2] L'Huillier A and Balcou P 1993 *Phys. Rev. Lett.* **70** 774
[3] Zhao J and Zhao Z X 2010 *Chin. Phys. Lett.* **27** 063301
[4] Wu Y Y, Dong Q L, Wang Z H, Liu P and Zhang J 2018 *Chin. Phys. Lett.* **35** 095201
[5] Gaumnitz T, Jain A, Pertot Y, Huppert M, Jordan I, Ardana-Lamas F and Wörner H J 2017 *Opt. Express* **25** 27506
[6] Itatani J, Levesque J, Zeidler D, Niikura H, Pépin H, Kieffer J C, Corkum P B and Villeneuve D M 2004 *Nature* **432** 867
[7] Zhang B, zhao J and Zhao Z X 2018 *Chin. Phys. Lett.* **35** 043201
[8] Ghimire S, Dichiara A D, Sistrunk E, Agostini P, Dimauro L F and Reis D A 2010 *Nat. Phys.* **7** 138
[9] Vampa G, McDonald C R, Orlando G, Klug D D, Corkum P B and Brabec T 2014 *Phys. Rev. Lett.* **113** 073901
[10] Jiang S, Chen J, Wei H, Yu C, Lu R and Lin C D 2018 *Phys. Rev. Lett.* **120** 253201
[11] Schubert O, Hohenleutner M, Langer F, Urbanek B, Lange C, Huttner U, Golde D, Meier T, Kira M and Koch S W 2014 *Nat. Photon.* **8** 119
[12] Hohenleutner M, Langer F, Schubert O, Knorr M, Huttner U, Koch S W, Kira M and Huber R 2015 *Nature* **523** 572
[13] Luu T T, Garg M, Kruchinin S Y, Moulet A, Hassan M T and Goulielmakis E 2015 *Nature* **521** 498
[14] Yu C, Zhang X, Jiang S, Cao X, Yuan G, Wu T, Bai L and Lu R 2016 *Phys. Rev. A* **94** 013846
[15] You Y S, Reis D A and Ghimire S 2017 *Nat. Phys.* **13** 345
[16] Liu H, Li Y, You Y S, Ghimire S, Heinz T F and Reis D A 2017 *Nat. Phys.* **13** 262
[17] Ndabashimiye G, Ghimire S, Wu M, Browne D A, Schafer K J, Gaarde M B and Reis D A 2016 *Nature* **534** 520
[18] Jin J Z, Xiao X R, Liang H, Wang M X, Chen S G, Gong Q and Peng L Y 2018 *Phys. Rev. A* **97** 043420
[19] Zhao K, Xu S Y, Jiang Y J and Wei Z Y 2018 *Acta Phys. Sin.* **67** 124203 (in Chinese)
[20] McDonald C R, Amin K S, Aalmalki S and Brabec T 2017 *Phys. Rev. Lett.* **119** 183902
[21] Osika E N, Chacón A, Ortmann L, Suárez N, Pérez-Hernández J A, Szafran B, Ciappina M F, Sols F, Landsman A S and Lewenstein M 2017 *Phys. Rev. X* **7** 021017
[22] Vampa G, Hammond T J, Thiré N, Schmidt B E, Légaré F, McDonald C R, Brabec T, Klug D D and Corkum P B 2015 *Phys. Rev. Lett.* **115** 193603
[23] Lanin A A, Stepanov E A, Fedotov A B and Zheltikov A M 2017 *Optica* **4** 516
[24] Tancogne-Dejean N, Mücke O D, Kärtner F X and Rubio A 2017 *Phys. Rev. Lett.* **118** 087403
[25] Meier T, von Plessen G, Thomas P and Koch S W 1994 *Phys. Rev. Lett.* **73** 902
[26] Golde D, Meier T and Koch S W 2006 *J. Opt. Soc. Am. B* **23** 2559
[27] Wu M, Ghimire S, Reis D A, Schafer K J and Gaarde M B 2015 *Phys. Rev. A* **91** 043839
[28] Korbman M, Kruchinin S Y and Yakovlev V S 2013 *New J. Phys.* **15** 013006
[29] Tamaya T, Ishikawa A, Ogawa T and Tanaka K 2016 *Phys. Rev. Lett.* **116** 016601
[30] Huttner U, Schuh K, Moloney J V and Koch S W 2016 *J. Opt. Soc. Am. B* **33** C22
[31] Corkum P B 1993 *Phys. Rev. Lett.* **71** 1994
[32] Lewenstein M, Balcou P, Ivanov M Y, L'Huillier A and Corkum P B 1994 *Phys. Rev. A* **49** 2117
[33] Vampa G, McDonald C R, Orlando G, Corkum P B and Brabec T 2015 *Phys. Rev. B* **91** 064302
[34] Guan Z, Zhou X X and Bian X B 2016 *Phys. Rev. A* **93** 033852
[35] Ghimire S, Ndabashimiye G, Dichiara A D, Sistrunk E, Stockman M I, Agostini P, Dimauro L F and Reis D A 2014 *J. Phys. B: At. Mol. Opt. Phys.* **47** 204030
[36] Zener C 1934 *Proceedings of the Royal Society of London A: Mathematical, Physical and Engineering Sciences* **145** 523
[37] Wu M, Browne D A, Schafer K J and Gaarde M B 2016 *Phys. Rev. A* **94** 063403
[38] Bloch F 1929 *Z. Phys.* **52** 555
[39] Mücke O D 2011 *Phys. Rev. B* **84** 081202
[40] Liu L, Zhao J, Dong W, Liu J, Huang Y and Zhao Z 2017 *Phys. Rev. A* **96** 053403
[41] Du T Y and Bian X B 2017 *Opt. Express* **25** 151
[42] Jia G R, Huang X H and Bian X B 2017 *Opt. Express* **25** 23654
[43] Wannier H G 1959 *Elements of Solid State Theory* (Cambridge: Cambridge University Press)
[44] Wannier G H 1960 *Phys. Rev.* **117** 432
[45] Mendez E E and Bastard G 1993 *Physics Today* **46** 34
[46] Mendez E E, Agulló-Rueda F and Hong J M 1988 *Phys. Rev. Lett.* **60** 2426
[47] Huang T, Zhu X, Li L, Liu X, Lan P and Lu P 2017 *Phys. Rev. A* **96** 043425
[48] Wang Z, Park H, Lai Y H, Xu J, Blaga C I, Yang F, Agostini P and Dimauro L F 2017 *Nat. Commun.* **8** 1
[49] Hansen K K, Bauer D and Madsen L B 2018 *Phys. Rev. A* **97** 043424
[50] Golde D, Meier T and Koch S W 2008 *Phys. Rev. B* **77** 075330
[51] McDonald C R, Vampa G, Corkum P B and Brabec T 2015 *Phys. Rev. A* **92** 033845
[52] Liu L, Zhao J, Yuan J and Zhao Z 2017 *Sci. Sin-Phys. Mech. Astron.* **47** 033006